applied sciences

MDPI

Article

Theranostic Investigation of Gadolinium-159 for Hepatocellular Carcinoma: Monte Carlo Simulation Study

Ahmed Sadeq Musa [1,2], Muhammad Fahmi Rizal Abdul Hadi [1], Nabeel Ibrahim Ashour [1,3] and Nurul Ab. Aziz Hashikin [1,*]

[1] School of Physics, Universiti Sains Malaysia, Penang 11800, Malaysia
[2] Department of Physiology and Medical Physics, College of Medicine, University of Kerbala, Kerbala 56001, Iraq
[3] Department of Physics, College of Science, University of Kerbala, Kerbala 56001, Iraq
* Correspondence: hashikin@usm.my

Abstract: Gadolinium-159 (^{159}Gd) is a beta emitter with appropriate energy for therapeutic application. However, this radioisotope additionally emits gamma rays, enabling the distribution of ^{159}Gd to be detected by a gamma camera after each therapeutic administration. The current research is innovative in the investigation of ^{159}Gd as a theranostic radioisotope in the radioembolization of HCC using Monte Carlo (MC) simulation. For ^{159}Gd therapeutic investigation, various patient scenarios including varying tumour involvement (TI), tumour-to-normal liver uptake ratio (T/N), and lung shunting (LS) were simulated using Geant4 MC to estimate the absorbed doses to organs at risk. For ^{159}Gd planar imaging investigation, the SPECTHead example from GATEContrib (GitHub) was utilized, and inside a liver a tumour was created and placed inside a torso phantom and simulated using GATE MC simulation. The majority of ^{159}Gd absorbed doses by normal liver and lungs were less than the maximum dose limitations of 70 Gy and 30 Gy, respectively. Absorbed doses to other organs were observed to be below 1 Gy. The utilization of 58 keV and 363.54 keV photopeaks in combination produced optimal planar imaging of ^{159}Gd. This research gives new insights into the use of ^{159}Gd as a theranostic radioisotope, with the potential to be used as an Yttrium-90 (^{90}Y) alternative for liver radioembolization.

Keywords: ^{159}Gd; Monte Carlo simulation; theranostic; Geant4; GATE; radioembolization; HCC

Citation: Musa, A.S.; Abdul Hadi, M.F.R.; Ashour, N.I.; Hashikin, N.A.A. Theranostic Investigation of Gadolinium-159 for Hepatocellular Carcinoma: Monte Carlo Simulation Study. *Appl. Sci.* **2022**, *12*, 12396. https://doi.org/10.3390/app122312396

Academic Editor: Ioanna Kyriakou

Received: 15 November 2022
Accepted: 2 December 2022
Published: 3 December 2022

1. Introduction

Hepatocellular Carcinoma (HCC) is one of the major causes of cancer-related deaths in the world [1]. Furthermore, liver cancer is the fourth most prevalent cause of cancer-related death, and the sixth most commonly diagnosed cancer [2]. Based on annual projections, the accumulated death caused by liver cancer will be more than one million by the year 2030, according to World Health Organization predictions [3]. However, in many countries, HCC morbidity and mortality are on the rise [4]. Currently, systemic drug treatments for HCC are limited, and side effects are prevalent [5]. There is a strong need to find other effective HCC treatment methods. The portal vein supplies most blood to normal liver tissue, whereas the hepatic artery supplies blood to most liver malignant tumours. As a result, locoregional therapies such as transarterial radioembolization (TARE) can be delivered preferentially in the arteries supporting tumours, resulting in particle deposition selectively in the tumour while avoiding detrimental side effects on healthy liver tissue [6]. Although radionuclides are increasingly used in nuclear medicine for both therapeutic and diagnostic purposes, precise patient-specific dosimetry is still not routinely conducted in clinical practice [7]. However, treatment planning for radioembolization of HCC might be challenging, because the amount of radiation that may be delivered to a tumour is restricted by the absorbed dose of organs at risk (OARs), which must be below the tolerable dose limit. Various MC codes can be used to simulate radiation transport over any media, providing

precise dose estimation. The MC program based on the GEometry ANd Tracking 4 (Geant4) simulation toolkit has been developed for medical radiation dosimetry applications [8]. Geant4 Application for Tomographic Emission (GATE) is one MC simulation software for nuclear medical imaging based on the Geant4 code used for nuclear imaging devices [9]. In gamma camera imaging, the acquisition energy window is centred around the photopeak to detect most primary photons. A well-established therapy option for hepatic radioembolization is the radioisotope, ^{90}Y, which provides beta radiation for therapy with the possibility of post-treatment imaging by bremsstrahlung radiation but with significantly poor quality [10], as the spectrum of bremsstrahlung radiation is both complicated and continuous; one of the most challenging topics in nuclear medicine is selecting acquisition energy windows [11]. Macroaggregated albumin (MAA) labelled with technetium-99m (^{99m}Tc) is currently employed as a radioactive tracer for planning ^{90}Y microsphere radioembolization therapy. It is critical to include this post-treatment imaging radioactive tracer in order to estimate the in vivo effects of ^{90}Y radiation [12]. Numerous theranostic (therapy and diagnostic) radioisotopes such as Samarium-153 (^{153}Sm), Holmium-166 (^{166}Ho), Lutetium-177 (^{177}Lu), and Rhenium-188 (^{188}Re) have been proposed as ^{90}Y alternatives for radioembolization of HCC [13].^{159}Gd has also been proposed for theranostic applications, however, has not been fully explored, especially in radioembolization of HCC. The ^{159}Gd radioisotope has a physical half-life of 18.48 h and emits β particles with energy of 970.5 keV, making it suitable for HCC therapeutic purposes. The ^{159}Gd gamma spectrum has two photopeaks (58 keV and 363.54 keV) [14], enabling the dose distribution of ^{159}Gd to be detected by a gamma camera and SPECT during TARE therapeutic administration for HCC. Furthermore, it is a highly paramagnetic element, useful in imaging via MRI. In addition, imaging properties of ^{159}Gd using gamma camera, SPECT and MRI assist in the evaluation of liver radioembolization toxicity and efficacy and also enable quantitative imaging assessment of the post-administration intrahepatic dose distribution—or, more precisely, on the proportion of dose absorbed by the tumour compared to the dose absorbed by healthy tissue. These agents may also be used to predict patient response and optimize a patient-specific therapeutic dose. The ^{159}Gd radioisotope offers a broader therapy option as a theranostic radioisotope in hepatic radioembolization for HCC. In the current work, a Geant4 MC simulation was employed in order to delineate the dosimetric investigation of ^{159}Gd in the context of HCC radioembolization when the advised 120 Gy dose [15] is administered to a tumour for various patient parameter combinations, i.e., TI, T/N, and LS. Moreover, GATE MC simulations were employed in order to investigate the feasibility of utilizing ^{159}Gd gamma scintigraphic imaging following hepatic radioembolization and to compare our findings with ^{99m}Tc scintigraphic imaging.

To the best of our knowledge, this is the first study that has conducted the investigation of ^{159}Gd as a theranostic radioisotope in hepatic radioembolization of HCC using MC simulation.

2. Materials and Methods

2.1. Absorbed Dose Calculation

MIRD-5 Phantom Geant4 MC Simulations

According to Pamphlet 5 of the Medical Internal Radiation Dose (MIRD), a mathematical hermaphrodite adult phantom (Figure 1) was used in this study, which consisted of entire anatomical organs [16], with male and female reproductive organs (testicles) and (ovaries and uterus). Female breasts were also incorporated into the phantom by adopting the breasts from [17]. The MIRD-5 phantom is made up of three different types of tissues with densities of bone 1.4862 g/cm^3, lung 0.2958 g/cm^3, and soft tissue 0.9869 g/cm^3.

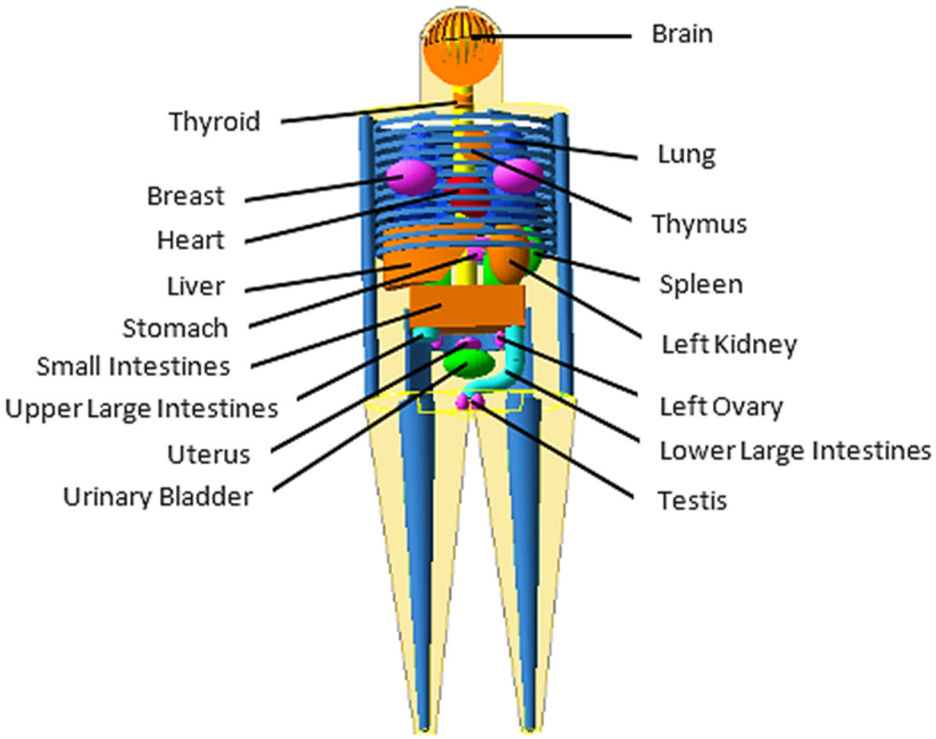

Figure 1. The MIRD-5 adult hermaphrodite human phantom as constructed and visualized using Geant4.

The Geant4 version 10. 6 toolkit was used in this study [18,19] as an advanced example human phantom. Within the liver, a single tumour was created with the same shape as the MIRD-5 mathematical liver, positioned in the centre and variable in mass (Figure 2). Equation (1) was used to calculate the tumour involvement $(TI)(\%)$.

$$Tumour\ Involvement\ (TI)(\%) = \frac{Mass\ of\ tumour}{Mass\ of\ liver} \times 100\% \quad (1)$$

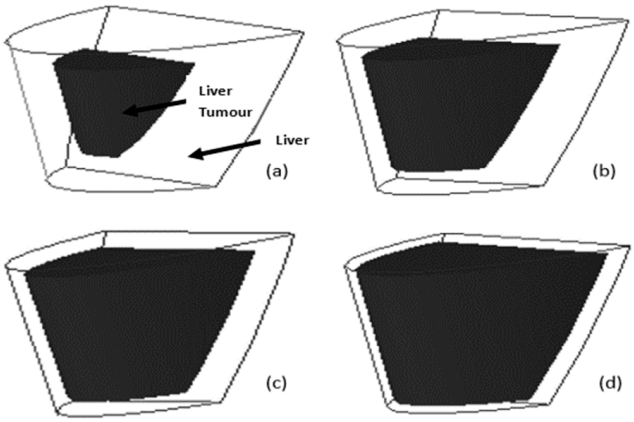

Figure 2. Antero-superior view of the tumour model for (**a**) 10, (**b**) 30, (**c**) 50, and (**d**) 70% tumour involvement (TI).

We used tumour shape as the shape of the mathematical MIRD-5 liver in this study. Due to the geometrical boundaries which were allowed, only spheres with a radius of up to 4.3 cm could be confined within the liver, resulting in a tumour mass of 333 g and a maximum tumour involvement of only 18.2% [13].

The electromagnetic interactions of photons and electrons were modelled using the low-energy electromagnetic package [20], which was based on the Livermore Evaluated Data Libraries. The generation threshold for secondary particles was set at one millimetre. The decay of ^{159}Gd and its distribution in the tumour, normal liver, lungs, and other organs were modelled using the Geant4 radioactive decay and general particle source components. The ^{159}Gd radionuclide point sources within each organ were evenly distributed, with activity uptake based on the T/N and LS, having emissions that are randomized in their direction. Normal liver, tumour, lungs, and other organs were set at sensitive volumes. The simulation's result was defined as mean energy (MeV) transferred into each volume. Several patient scenarios, including varying TI (10, 30, 50, and 70%), LS (0, 5, 10, 15, and 20%), and T/N (1, 2.5, 5, 7.5, and 10) were simulated. The Geant4 MC package was used to simulate the setup with 10^7 histories. The simulation was run thrice for each parameter combination to achieve a less than 1% standard deviation. To obtain a tumour dose of 120 Gy, the tumour, normal liver, lungs, and other organ doses acquired via simulation were multiplied by the same factor that provides a tumour dose of 120 Gy. When a recommended dose of 120 Gy [15] was delivered to the tumour, the absorbed dose (Gy) to normal liver, lungs, and other organs was calculated by converting the mean energy (MeV) transferred within the organs to joules (J) and dividing it by the mass of the organ.

2.2. Scintigraphic Imaging

2.2.1. GATE MC Simulation

GATE is a widely used MC simulation platform, comprising a general-purpose code called Geant4 and advanced open-source called OpenGATE, first publicly released in 2004 by the OpenGATE international collaboration (Los Angeles, CA, USA) [21]. Many studies have confirmed the platform's usefulness, accuracy, and effectiveness [21–24]. This study runs simulations on an open-source Debian-based Linux distribution using the latest long-term support (Ubuntu 18.04 LTS) using an Intel Xeon Gold 6242 (16 cores, 32 threads) with Geant4 version 10.6 p.01, ROOT 6.14/06, and GATE version 9.1 installed. We used the Geant4 with code including electromagnetic physics list option four as a physics list with one millimetre cut off. The setup was simulated via the GATE MC package, with histories of 10^9. The SPECTHead example obtained from the GATEContrib (GitHub, San Francisco, CA, USA) was used in order to construct representative geometry for the current work.

2.2.2. Geometry Setup

The geometry was configured to engineer a trapezoid liver, with a density of 0.9869 g/cm^3, containing a spherically shaped tumour with a 1 cm diameter. This combination was inserted into a cylindrical torso phantom as shown in Figure 3.

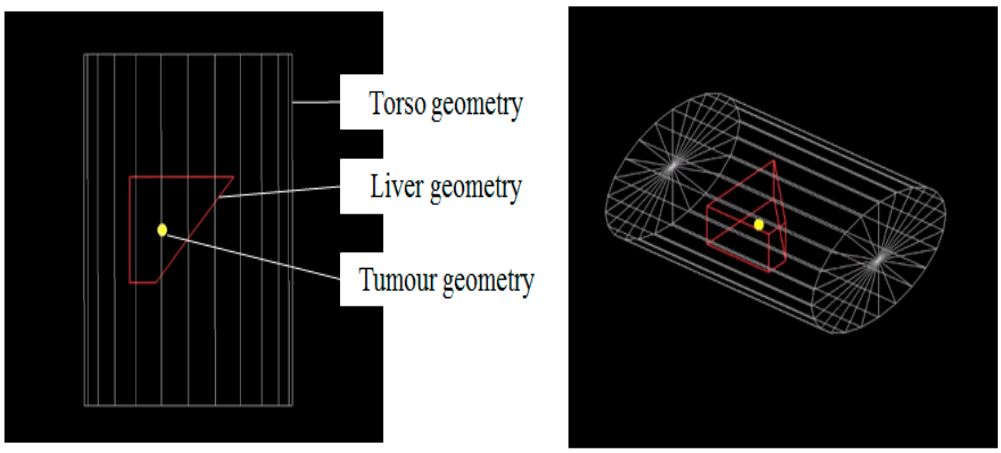

Figure 3. Geometrical configuration of the cylindrical torso phantom containing liver and tumour.

2.2.3. Image Acquisition

A gamma head (with NaI detector) was modelled for image acquisition using the SPECTHead example from GateContrib (GitHub) [25], with dimensions of 21 × 30 × 13 cm^3 and a position of 3.5 cm from the phantom's centre as shown in Figure 4. The ^{159}Gd and ^{99m}Tc sources were simulated separately, and for image acquisition were distributed uniformly throughout the liver and tumour volumes (assuming a tumour-to-normal liver ratio of 2:1). For the simulation, the matrix size was set at 256 × 256. The ^{159}Gd and ^{99m}Tc necessitated employing high-energy general-purpose (HEGP) and low-energy high-resolution (LEHR) collimators, respectively, the properties of which are presented in Table 1. The primary energy windows for ^{159}Gd included 20% photopeaks at 58 keV (46.4–69.6 keV) and 363.54 keV (290.8–436.2 keV); for ^{99m}Tc, a 10% photopeak at 140 keV (126–154 keV) was used. During the simulation, acquisition of the individual images was performed over a minimum of 10 K counts.

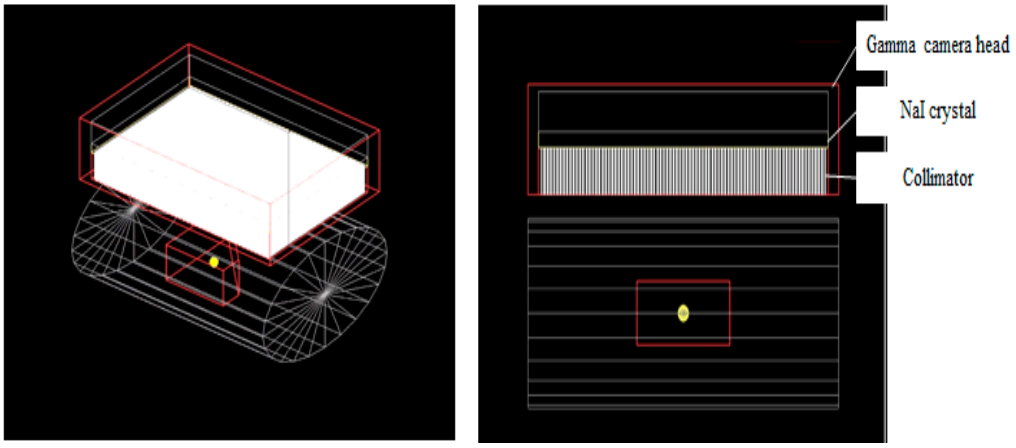

Figure 4. Geometry setup of gamma camera and phantom. Yellow dots represent the tumour.

Table 1. Characteristics of collimators used for ^{159}Gd and ^{99m}Tc.

Radioisotope	Collimator	Length (mm)	Septal Thickness (mm)	Hole Diameter (mm)
^{159}Gd	High-energy general purpose (HEGP)	60	2	4
^{99m}Tc	Low-energy high-resolution (LEHR)	24.05	0.160	1.11

2.2.4. Image Quality Analysis Using ImageJ

Once the simulations were complete, the output of simulation file format (planar.mhd) underwent importation into the software, ImageJ, version 1.53c, in order to assess image quality. The latter was determined following computation of the signal: background ratio (*SBR*) and the coefficient of variation (*CV*).

$$SBR = \frac{mean\ pixel\ count\ of\ tumour}{mean\ pixel\ count\ of\ background} \quad (2)$$

$$CV = \frac{standard\ deviation\ count\ of\ tumour}{mean\ pixel\ count\ of\ tumour} \quad (3)$$

A region of interest (ROI) was created within the tumour, which enabled mean pixel value and standard deviation to be acquired. Copies of the tumour ROI were then applied to three different background locations within the visible liver region, as shown in Figure 5. The mean and standard deviation values were again taken. The SBR and CV were obtained by using Equations (2) and (3) [26], respectively.

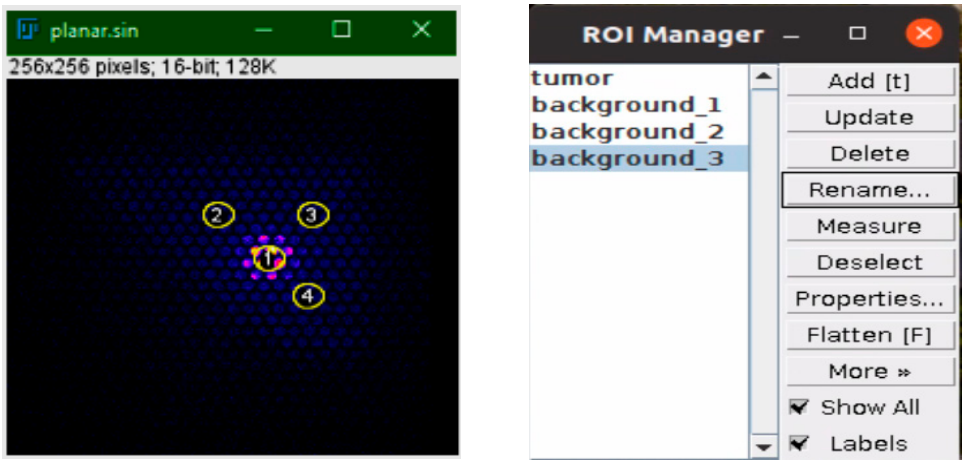

Figure 5. Example of ImageJ software used to assess the quality of liver and tumour planar images. Yellow circles (1, 2, 3, 4) represent the region of interest.

3. Results and Discussion

3.1. Absorbed Dose to Normal Liver

When the tumour received 120 Gy, the range of normal liver absorbed doses from ^{159}Gd is between 12.98 and 117.49 Gy for all parameter combinations of TI, LS, and T/N (Figure 6). Moreover, the absorbed doses exceeded the acceptable dose limit of normal liver (i.e., 70 Gy) [15,27] only at a T/N of 1 because the sources in the liver and tumour are similar and cause higher doses.

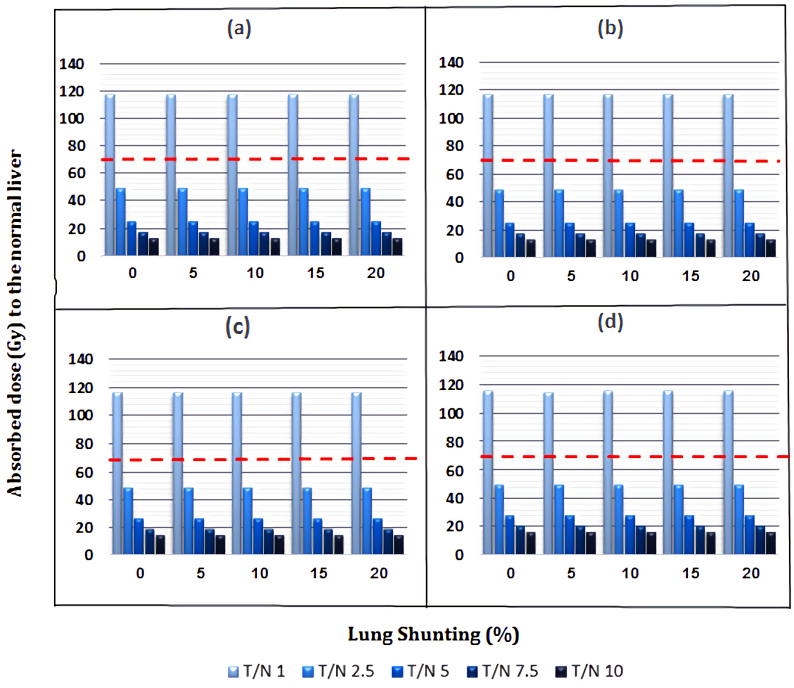

Figure 6. Absorbed dose to the normal liver for various TIs of (**a**) 10, (**b**) 30, (**c**) 50, and (**d**) 70%, LS, and T/N, when 120 Gy is delivered to the tumour. The red dotted lines represent the maximum dose limit of 70 Gy for a normal liver.

3.2. Absorbed Dose to Lungs

When the tumour received 120 Gy, the range of the left and right lung absorbed doses was between 0.019 and 51.39 Gy, respectively, and 0.11 to 51.86 Gy for all parameter combinations of TI, LS, and T/N (Figures 7 and 8). In terms of comparison, the doses were

slightly higher in the right lung because it was closer to liver. Furthermore, the absorbed doses by the lungs exceeded the acceptable dose limit of lungs (i.e., 30 Gy) [28,29] at 15% LS with a T/N of 1 (for all TI) and 20% LS with various T/Ns: 1 (for all TI), 2.5 (30, 50, and 70% TI), 5 (50 and 70% TI), 7.5, and 10 (both for 70% TI).

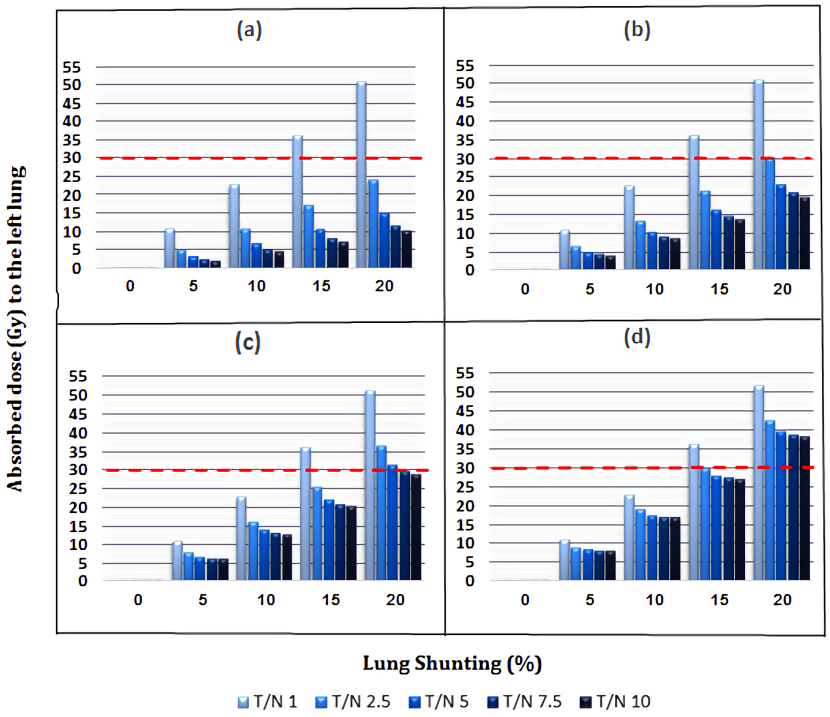

Figure 7. Absorbed dose to the left lung for various TIs of (**a**) 10, (**b**) 30, (**c**) 50, and (**d**) 70%, LS, and T/N, when 120 Gy is delivered to the tumour. The red dotted lines indicate the maximum dose limit to lungs of 30 Gy.

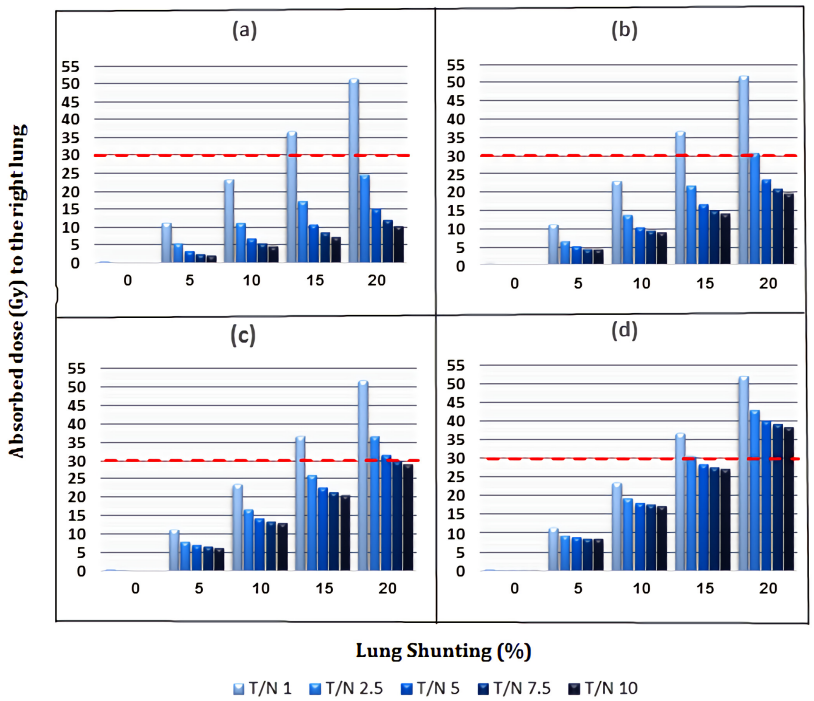

Figure 8. Absorbed dose to the right lung for various TIs of (**a**) 10, (**b**) 30, (**c**) 50, and (**d**) 70%, LS, and T/N, when 120 Gy is delivered to the tumour. The red dotted lines indicate the maximum dose limit to lungs of 30 Gy.

3.3. Absorbed Dose to Other Organs

In order to estimate the absorbed dose from ^{159}Gd to other organs when 120 Gy is delivered to the tumour, we selected the parameter combinations which have higher impacts on the absorbed dose: TI (70%), LS (20%), and T/N (1), as illustrated in Figure 9.

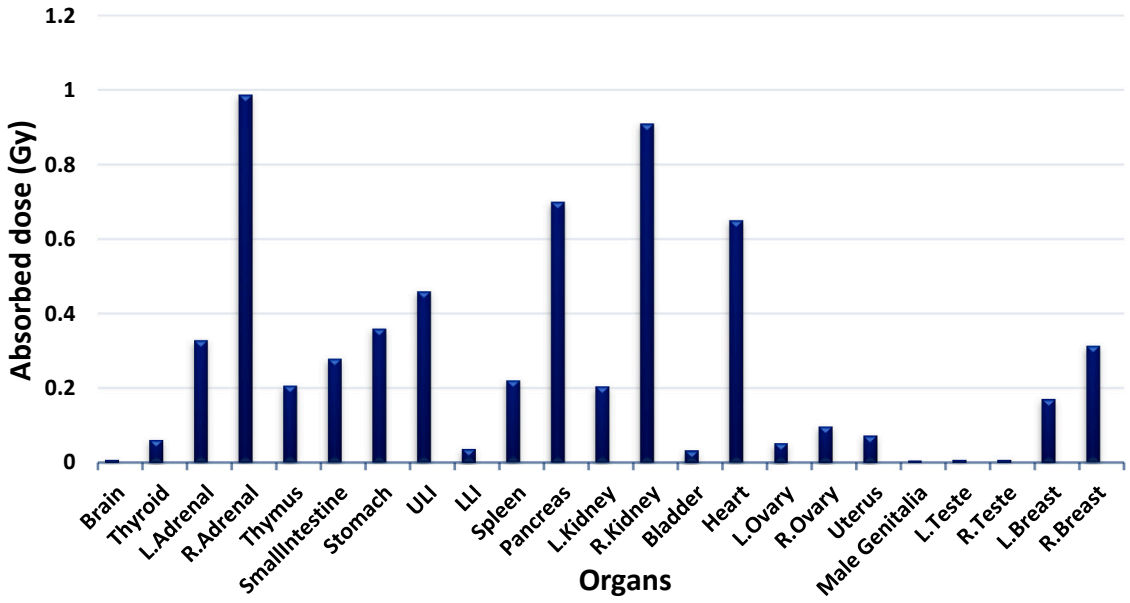

Figure 9. Absorbed dose to other organs for tumour involvement of 70%, lung shunting (LS) (20%), and tumour to normal liver uptake ratio (T/N) 1, when 120 Gy is delivered to the tumour. L: left, R: right, ULI: upper large intestines, LLI: lower large intestines.

The outcome following radioembolization is predominantly linked to the radiation dose absorbed by normal liver, lungs, and other organs [30]. As radiation oncologists carry out hepatic brachytherapy on a routine basis, they should have an empirical comprehension of the absorbed dose which reaches the tumour [31]. This is paramount in order to maximize the radiation received by the tumour and to reduce the collateral damage to normal tissue as much as possible. Previously, hepatic radioembolization has been applied without a precise appreciation of the respective quantities of radiation absorbed by the normal liver, lungs, and other organs [32,33]. From this study, it has been observed that the absorbed dose to the normal liver is primarily dependent on T/N because when T/N increases, the absorbed doses of the normal liver decrease due to the lower administered activity required to deliver the 120 Gy tumour dose [34] and not due to TI and LS (Figure 6). The absorbed dose to left and right lungs are impacted by all three factors， i.e., TI, LS, and T/N; and LS was the most influential parameter [35] as illustrated in Figures 7 and 8. Figure 9 show the absorbed doses from gamma emission to the other organs which are similar in shape and equal in mass; it is clearly observed that organs located on the same side as the liver (right side of the body) absorb a higher dose than organs located on the left side according to the inverse square law, and the absorbed dose to other organs decreases as the distance from the liver increases [36]. The highest absorbed dose was found in the right adrenal because it is located just below the liver. Despite the fact that the right and left adrenals are roughly equal in mass, the right adrenal absorbs a significantly higher dose than the left adrenal due to their unequal distance from the liver, as shown in Figure 9. Results demonstrate that ^{159}Gd gamma emission is not risky and is completely safe, and that the treatment is not restricted by the absorbed dose received by other organs. This is because when 120 Gy is delivered to the tumour, all other organs' absorbed doses were below 1 Gy or only less than 1% as compared to the absorbed dose given to the tumour. This was supported by

dosimetric research for radioembolization with Holmium-166 microspheres, which found that the gamma emission contributed just 1.1% of the overall absorbed dose [37].

The ^{90}Y, ^{166}Ho, ^{153}Sm, and ^{177}Lu radioisotopes have been studied and investigated by Hashikin et al. (2016) using the MIRD phantom. However, in their study it was concluded that the total estimated tumour dose for all radionuclides was 262.9 Gy. Furthermore, the tumour dose of 1.82 GBq ^{90}Y has been obtained, whereby ^{153}Sm, ^{166}Ho, and ^{177}Lu obtained same tumour doses at 8.32, 5.83, and 4.44 GBq, respectively. In terms of comparison, the normal liver doses of the other radionuclides were lower than ^{90}Y, which was advantageous for sparing normal tissue. Interestingly, even though the other organ doses from ^{153}Sm and ^{177}Lu were higher due to higher gamma energy, they were still below 1 Gy. They show promise as ^{90}Y substitutes, delivering comparable tumour doses, reduced normal liver and lung doses, and doses absorbed by other organs considerably below the tolerance limit [13]. In our study, we obtained similar results when the recommended therapeutic dose from ^{159}Gd was given to the tumour, as all other organs' absorbed doses were below 1 Gy, as illustrated in Figure 9.

3.4. ^{159}Gd vs. ^{99m}Tc Scintigraphic Imaging

The GATE MC simulation for ^{99m}Tc and different photopeaks of ^{159}Gd were conducted separately, the output of the simulation (file format planar.mhd) was imported into the software VV Image Viewer version 1.4 to obtain the planar images, as illustrated in Figure 10.

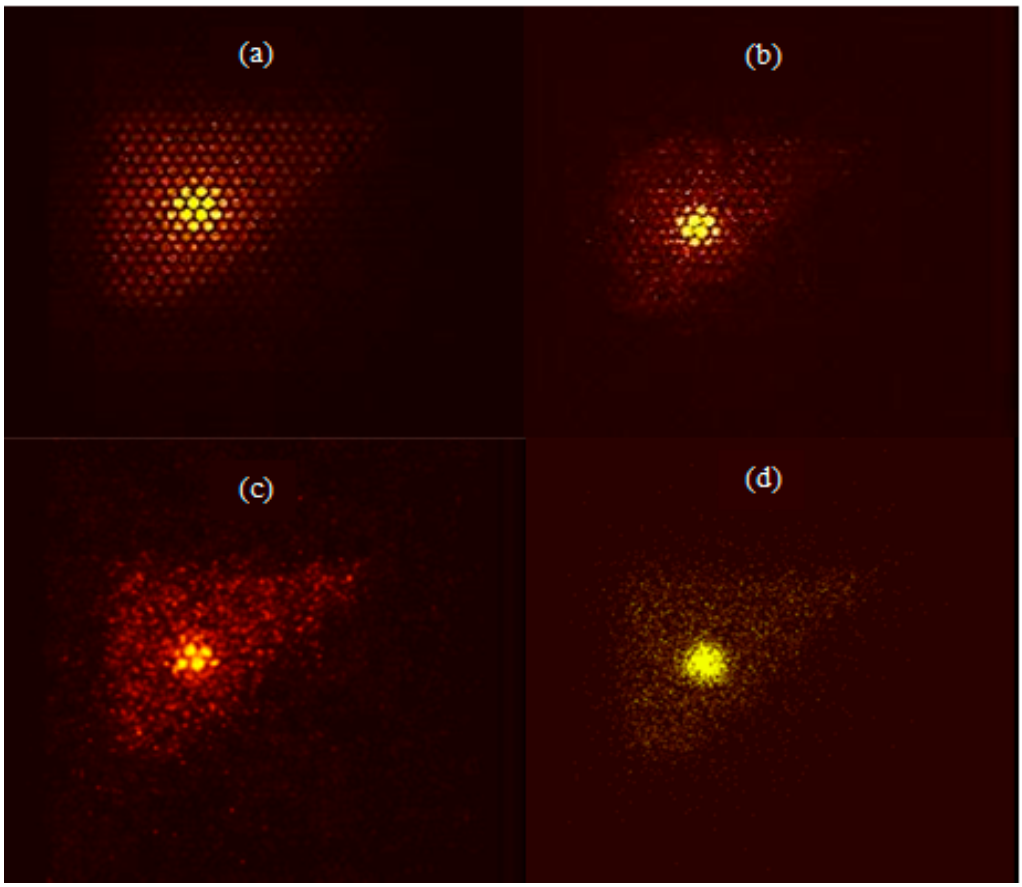

Figure 10. Planar image acquired from GATE MC simulation for ^{159}Gd and ^{99m}Tc utilizing VV image viewer: (**a**) ^{159}Gd (58 + 363.54 keV), (**b**) ^{159}Gd (58 keV), (**c**) ^{159}Gd (363.54 keV), and (**d**) ^{99m}Tc (140 keV).

Figures 11 and 12 demonstrate the gamma spectra of ^{159}Gd and ^{99m}Tc detected from the root file of the GATE MC simulation; ROOT software version 6.26/10 was used for this process.

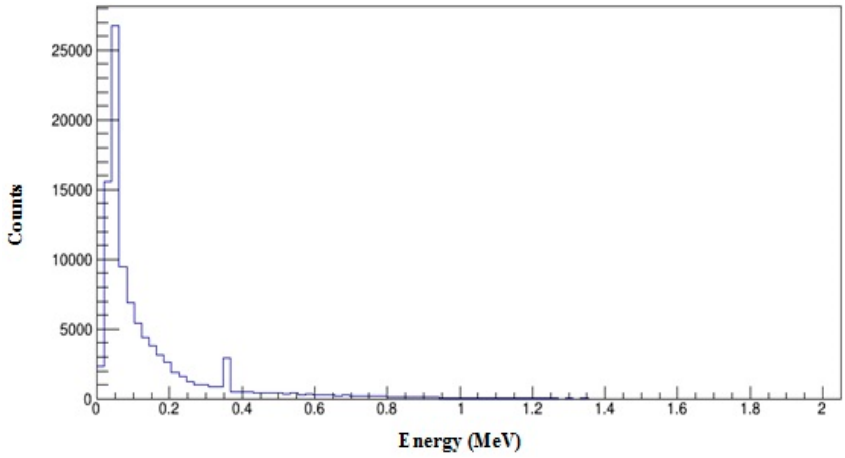

Figure 11. Gamma spectrum for ^{159}Gd detected from output GATE MC simulation root file, using ROOT software.

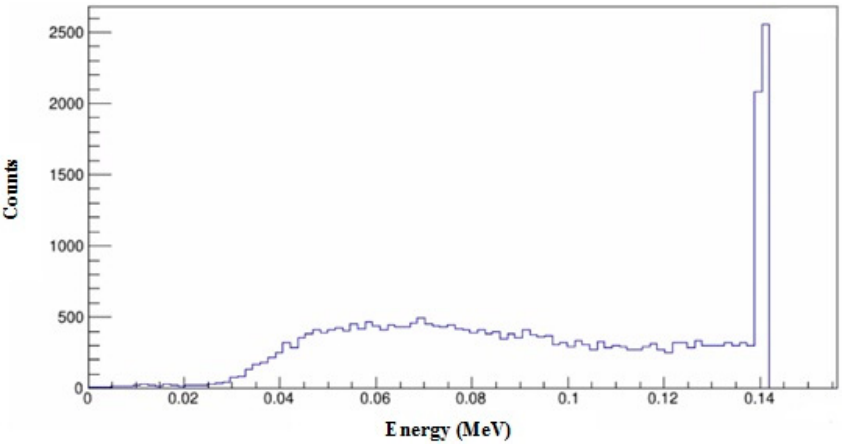

Figure 12. Gamma spectrum for ^{99m}Tc detected from output GATE MC simulation root file, using ROOT software.

The quality assessment of planar images obtained using ImageJ software for ^{99m}Tc and different photopeaks of ^{159}Gd were determined using Equations (2) and (3) to compute SBR and CV, as demonstrated in Figures 13 and 14.

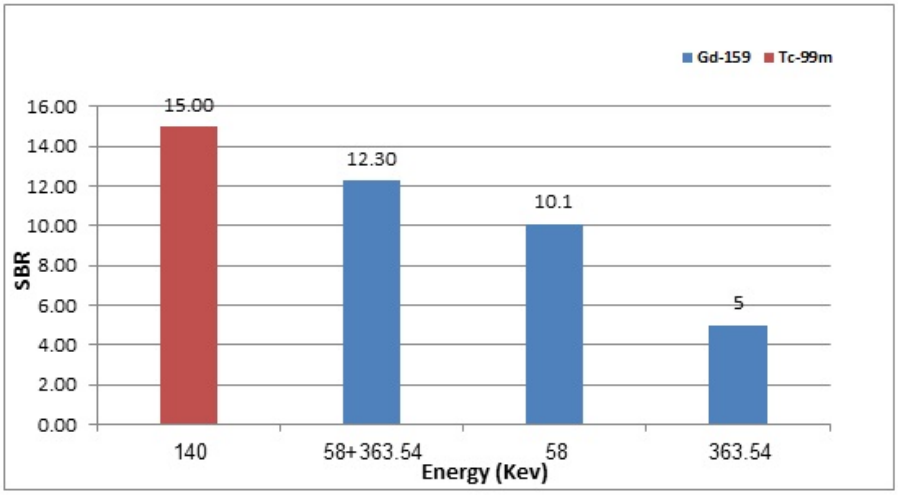

Figure 13. Signal to background ratio for the image acquired from ^{99m}Tc and different photopeaks of ^{159}Gd using ImageJ software.

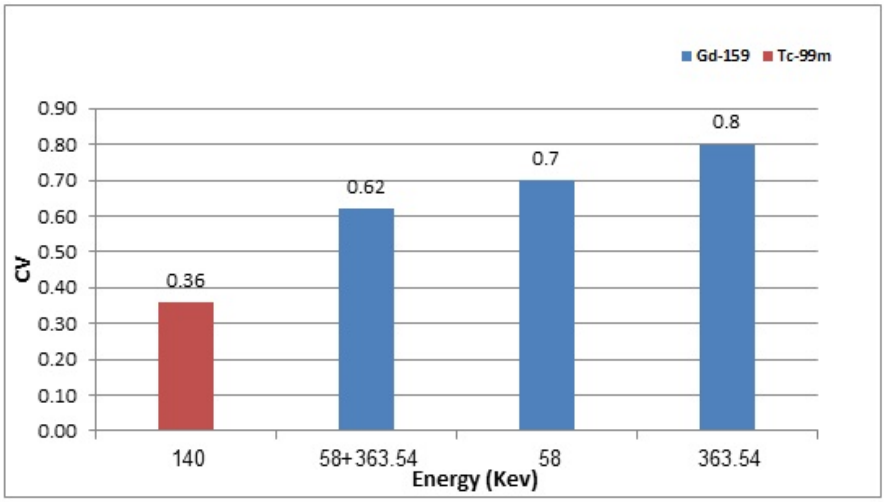

Figure 14. Coefficient of variation for the image acquired from ^{99m}Tc and different photopeaks of ^{159}Gd using ImageJ software.

The beta-emitting characteristics of ^{159}Gd ensure that it is an efficacious radioisotope for cancer oncotherapeutic applications [38–41]. Radioembolization procedures of liver tumours necessitate quantitative imaging following therapy [42]. Currently, there are no studies regarding the use of ^{159}Gd as a theranostic radioisotope in this context. We used GATE MC simulation in this study to investigate the scintigraphic imaging possibility of ^{159}Gd for hepatic radioembolization. The ^{159}Gd photopeak selection was 58 vs. 363.54 vs. 58 + 363.54 keV. Figure 13 shows that the image quality using both photopeaks combined (58 + 363.54 keV) is better with the highest SBR; a higher SBR indicates that the images can provide superior spatial information. Figure 14 shows that the lowest CV is obtained using both photopeaks combined (58 + 363.54 keV); a lower CV indicates minor variation (better estimation). This observation can be explained by combining two photopeaks resulting in the highest count statistics. The hexagonal hole pattern of the collimator is visible in the ^{159}Gd acquired planar image because of ^{159}Gd emitting high-energy gamma rays, the thicker septa, and the larger hole size of the HEGP collimator used [43,44] (Figure 10). The 58 keV photopeak of the ^{159}Gd gamma spectrum appears with significantly higher intensity than expected based on its emission intensities (Figure 11), because low-energy photons are more likely to penetrate the HEGP collimator's larger hole size. In comparison to ^{99m}Tc, in the ^{159}Gd planar image acquired using the two photopeaks in combination, SBR for ^{99m}Tc was 19.7% higher than for ^{159}Gd (Figure 13); CV was 53% lower than for ^{159}Gd (Figure 14).

Bouzekraoui et al. (2019) employed the SIMIND Monte Carlo simulation code using ^{159}Gd to determine the energy windows for the triple energy window (TEW) scatter correction approach. However, it has been observed that 20% of the main energy windows with 3 and 6 keV sub-energy windows were best for the TEW method implementation in ^{159}Gd [45]. Furthermore, a similar pattern of results was obtained in our study, which found that using two energy windows during acquisition admits better planar image quality results than using a single peak energy window, as illustrated in Figures 13 and 14, respectively.

The research findings suggest completing the following study phases, where cell cultures (in vitro) and animal experiments (in vivo) can be investigated to supplement the trials before moving into the clinical phase.

4. Conclusions

In this study, we showed that ^{159}Gd beta particle emission provides the recommended therapeutic dose of 120 Gy to tumours while maintaining the permissible absorbed dose of a normal liver (70 Gy) [15,27] and for lungs (30 Gy) [28,29]. Additionally, the treatment is not restricted by the gamma emission absorbed dose received by other organs, because when

120 Gy was delivered to the tumour, all other organs' absorbed doses were below 1 Gy [13] or less than 1% as compared to the absorbed dose given to the tumour [37]. Furthermore, the combination of 58 keV and 363.54 keV gamma energy photopeaks produced optimal planar imaging of ^{159}Gd. Hence, ^{159}Gd offers a broader therapy option for HCC with increased availability and perhaps lower treatment costs. In conclusion, this study gives new insights into the use of ^{159}Gd as a theranostic radioisotope with the potential to be used as a ^{90}Y alternative for liver radioembolization.

Author Contributions: A.S.M. and N.A.A.H. conceived the idea. N.A.A.H. supervised all the simulations and analyses. A.S.M., M.F.R.A.H. and N.I.A. performed software characterizations, measurements, and analysed the results. N.A.A.H. commented on manuscript writing. A.S.M. wrote the manuscript. All authors discussed the results and commented on the manuscript of the work. All authors have read and agreed to the published version of the manuscript.

Funding: The authors acknowledge the Ministry of Higher Education Malaysia for the Fundamental Research Grant Scheme (FRGS/1/2019/STG02/USM/02/2) for the financial support in conducting this research.

Institutional Review Board Statement: Not applicable.

Informed Consent Statement: Not applicable.

Data Availability Statement: Not applicable.

Acknowledgments: The authors would also like to thank School of Physics, Universiti Sains Malaysia, for supporting this research work.

Conflicts of Interest: The authors declare no conflict of interest.

Abbreviations

^{159}Gd	Gadolinium-159
^{90}Y	Yttrium-90
MC	Monte Carlo
HCC	Hepatocellular Carcinoma
TI	Tumour involvement
T/N	Tumour-to-normal liver uptake ratio
LS	Lung shunting
TARE	Transarterial radioembolization
OARs	Organs at risk
GATE	Geant4 Application for Tomographic Emission
Geant4	GEometry ANd Tracking
^{99m}Tc	Technetium-99m
^{153}Sm	Samarium-153
^{166}Ho	Holmium-166
^{177}Lu	Lutetium-177
^{188}Re	Rhenium-188
MRI	Magnetic resonance imaging
SPECT	Single-photon emission computed tomography
MIRD	Medical Internal Radiation Dose
HEGP	High-energy general-purpose
LEHR	Low-energy high-resolution
SBR	Signal to background ratio
CV	Coefficient of variation
ROI	Region of interest

References

1. Villanueva, A. Hepatocellular Carcinoma. *N. Engl. J. Med.* **2019**, *380*, 1450–1462. [CrossRef] [PubMed]
2. World Health Organization. *International Agency for Research on Cancer Cancer today*; World Health Organization: Geneva, Switzerland, 2016.

3. World Health Organization. *Projections of Mortality and Causes of Death, 2016 to 2060*; World Health Organization: Geneva, Switzerland, 2019. Available online: http://www.who.int/healthinfo/global_burden_disease/projections/en/ (accessed on 14 October 2018).
4. Liu, Z.; Jiang, Y.; Yuan, H.; Fang, Q.; Cai, N.; Suo, C.; Jin, L.; Zhang, T.; Chen, X. The trends in incidence of primary liver cancer caused by specific etiologies: Results from the Global Burden of Disease Study 2016 and implications for liver cancer prevention. *J. Hepatol.* **2019**, *70*, 674–683. [CrossRef] [PubMed]
5. Cidon, E.U. Systemic treatment of hepatocellular carcinoma: Past, present and future. *World J. Hepatol.* **2017**, *9*, 797–807. [CrossRef] [PubMed]
6. Gates, V.L.; Atassi, B.; Lewandowski, R.J.; Ryu, R.K.; Sato, K.T.; A Nemcek, A.; Omary, R.; Salem, R. Radioembolization with Yttrium-90 microspheres: Review of an emerging treatment for liver tumors. *Future Oncol.* **2007**, *3*, 73–81. [CrossRef] [PubMed]
7. Stabin, M. Nuclear medicine dosimetry. *Phys. Med. Biol.* **2006**, *51*, R187. [CrossRef]
8. Gholami, S.; Longo, F.; Nedaie, H.A.; Berti, A.; Mousavi, M.; Meigooni, A.S. Application of Geant4 Monte Carlo simulation in dose calculations for small radiosurgical fields. *Med. Dosim.* **2018**, *43*, 214–223. [CrossRef]
9. Jan, S.; Santin, G.; Strul, D.; Staelens, S.; Assié, K.; Autret, D.; Avner, S.; Barbier, R.; Bardies, M.; Bloomfield, P.M.; et al. GATE: A simulation toolkit for PET and SPECT. *Phys. Med. Biol.* **2004**, *49*, 4543–4561. [CrossRef]
10. Shen, S.; DeNardo, G.L.; Yuan, A.; A DeNardo, D.; DeNardo, S.J. Planar gamma camera imaging and quantitation of yttrium-90 bremsstrahlung. *J. Nucl. Med.* **1994**, *35*, 1381–1389.
11. Rong, X.; Du, Y.; Ljungberg, M.; Rault, E.; Vandenberghe, S.; Frey, E.C. Development and evaluation of an improved quantitative 90Y bremsstrahlung SPECT method. *Med. Phys.* **2012**, *39*, 2346–2358. [CrossRef]
12. Wright, C.L.; Zhang, J.; Tweedle, M.F.; Knopp, M.V.; Hall, N.C. Theranostic imaging of Yttrium-90. *BioMed Res. Int.* **2015**, *2015*, 481279. [CrossRef]
13. Hashikin, N.; Yeong, C.H.; Guatelli, S.; Abdullah, B.J.J.; Ng, K.H.; Malaroda, A.; Rosenfeld, A.B.; Perkins, A.C. Organ Doses from Hepatic Radioembolization with 90Y, 153Sm, 166Ho and 177Lu: A Monte Carlo Simulation Study Using Geant4. *J. Phys. Conf. Ser.* **2016**, *694*, 012059. [CrossRef]
14. Bé, M.M.; Chechev, V.P. Recommended standards for gamma ray intensities. *Nucl. Instrum. Methods Phys. Res. A Accel. Spectrom. Detect. Assoc. Equip.* **2013**, *728*, 157–172. [CrossRef]
15. Lau, W.-Y.; Kennedy, A.S.; Kim, Y.H.; Lai, H.K.; Lee, R.-C.; Leung, T.W.; Liu, C.-S.; Salem, R.; Sangro, B.; Shuter, B.; et al. Patient selection and activity planning guide for selective internal radiotherapy with yttrium-90 resin microspheres. *Int. J. Radiat. Oncol. Biol. Phys.* **2012**, *82*, 401–407. [CrossRef] [PubMed]
16. Snyder, W. Estimates of specific absorbed fractions for monoenergetic photon sources uniformly distributed in various organs of a heterogeneous phantom. *MIRD Pam.* **1978**, *5*, 10025874511.
17. Cristy, M.; Eckerman, K. *Specific Absorbed Fractions of Energy at Various Ages from Internal Photon Sources: 1, Methods*; Oak Ridge National Laboratory: Oak Ridge, TN, USA, 1987.
18. Allison, J.; Amako, K.; Apostolakis, J.; Araujo, H.; Dubois, P.A.; Asai, M.; Barrand, G.; Capra, R.; Chauvie, S.; Chytracek, R.; et al. Geant4 developments and applications. *IEEE Trans. Nucl. Sci.* **2006**, *53*, 270–278. [CrossRef]
19. Agostinelli, S.; Allison, J.; Amako, K.; Apostolakis, J.; Araujo, H.; Arce, P.; Asai, M.; Axen, D.; Banerjee, S.; Barrand, G.; et al. GEANT4—A simulation toolkit. *Nucl. Instrum. Methods Phys. Res. A Accel. Spectrom. Detect. Assoc. Equip.* **2003**, *506*, 250–303. [CrossRef]
20. Chauvie, S.; Guatelli, S.; Ivanchenko, V.; Longo, F.; Mantero, A.; Mascialino, B.; Nieminen, P.; Pandola, L.; Parlati, S.; Peralta, L.; et al. Geant4 Low Energy Electromagnetic Physics. In Proceedings of the IEEE Symposium Conference Record Nuclear Science, Rome, Italy, 16–22 October 2004.
21. Jan, S.; Benoit, D.; Becheva, E.; Carlier, T.; Cassol, F.; Descourt, P.; Frisson, T.; Grevillot, L.; Guigues, L.; Maigne, L.; et al. GATE V6: A major enhancement of the GATE simulation platform enabling modelling of CT and radiotherapy. *Phys. Med. Biol.* **2011**, *56*, 881–901. [CrossRef]
22. Konik, A.; Madsen, M.T.; Sunderland, J.J. GATE simulations of small animal SPECT for determination of scatter fraction as a function of object size. *IEEE Trans. Nucl. Sci.* **2012**, *59*, 1887–1891. [CrossRef]
23. Stute, S.; Carlier, T.; Cristina, K.; Noblet, C.; Martineau, A.; Hutton, B.; Barnden, L.; Buvat, I. Monte Carlo simulations of clinical PET and SPECT scans: Impact of the input data on the simulated images. *Phys. Med. Biol.* **2011**, *56*, 6441–6457. [CrossRef]
24. Lazaro, D.; Buvat, I.; Loudos, G.; Strul, D.; Santin, G.; Giokaris, N.; Donnarieix, D.; Maigne, L.; Spanoudaki, V.; Styliaris, S.; et al. Validation of the GATE Monte Carlo simulation platform for modelling a CsI (Tl) scintillation camera dedicated to small-animal imaging. *Phys. Med. Biol.* **2004**, *49*, 271. [CrossRef]
25. Available online: https://github.com/OpenGATE/GateContrib (accessed on 16 August 2022).
26. Huey, O.S.; See, Y.J.; Nabila, S.; Ping, H.S.; Suzanah, I. Collimator and energy window optimization for practical imaging protocol and quantification of Yttrium-90 bremsstrahlung spect/ct: A phantom study. *Radiat. Phys. Chem.* **2021**, *178*, 109080. [CrossRef]
27. Sirtex Medical Inc. *Sirtex Medical Training Manual. Training Program: Physicians and Institutions*; SIRTeX Medical Limited: Woburn, MA, USA, 2015.
28. Garin, E.; Rolland, Y.; Laffont, S.; Edeline, J. Clinical impact of 99m Tc-MAA SPECT/CT-based dosimetry in the radioembolization of liver malignancies with 90 Y-loaded microspheres. *Eur. J. Nucl. Med. Mol. Imaging* **2016**, *43*, 559–575. [CrossRef] [PubMed]

29. Ho, S.; Lau, W.Y.; Leung, T.W.T.; Chan, M.; Johnson, P.J.; Li, A.K.C. Clinical evaluation of the partition model for estimating radiation doses from yttrium-90 microspheres in the treatment of hepatic cancer. *Eur. J. Nucl. Med.* **1997**, *24*, 293–298. [PubMed]
30. Memon, K.; Lewandowski, R.J.; Kulik, L.; Riaz, A.; Mulcahy, M.F.; Salem, R. Radioembolization for Primary and Metastatic Liver Cancer. In *Seminars in Radiation Oncology*; Elsevier: Amsterdam, The Netherlands, 2011.
31. Sarfaraz, M.; Kennedy, A.S.; Cao, Z.J.; Sackett, G.D.; Yu, C.X.; Lodge, M.A.; Murthy, R.; Line, B.R.; Van Echo, D.A. Physical aspects of yttrium-90 microsphere therapy for nonresectable hepatic tumors. *Med. Phys.* **2003**, *30*, 199–203. [CrossRef] [PubMed]
32. Vilgrain, V.; Pereira, H.; Assenat, E.; Guiu, B.; Ilonca, A.D.; Pageaux, G.-P.; Sibert, A.; Bouattour, M.; Lebtahi, R.; Allaham, W.; et al. Efficacy and safety of selective internal radiotherapy with yttrium-90 resin microspheres compared with sorafenib in locally advanced and inoperable hepatocellular carcinoma (SARAH): An open-label randomised controlled phase 3 trial. *Lancet Oncol.* **2017**, *18*, 1624–1636. [CrossRef]
33. Helmberger, T.; Golfieri, R.; Pech, M.; Pfammatter, T.; Arnold, D.; Cianni, R.; Maleux, G.; Munneke, G.; Pellerin, O.; Peynircioglu, B.; et al. Clinical application of trans-arterial radioembolization in hepatic malignancies in europe: First results from the prospective multicentre observational study CIRSE registry for SIR-spheres therapy (CIRT). *Cardiovasc. Interv. Radiol.* **2021**, *44*, 21–35. [CrossRef] [PubMed]
34. Gulec, S.A.; Mesoloras, G.; Stabin, M. Dosimetric techniques in 90Y-microsphere therapy of liver cancer: The MIRD equations for dose calculations. *J. Nucl. Med.* **2006**, *47*, 1209–1211.
35. Kao, Y.H.; Magsombol, B.M.; Toh, Y.; Tay, K.H.; Chow, P.K.; Goh, A.S.W.; Ng, D.C.E. Personalized predictive lung dosimetry by technetium-99m macroaggregated albumin SPECT/CT for yttrium-90 radioembolization. *EJNMMI Res.* **2014**, *4*, 1–12. [CrossRef]
36. Marcié, S.; Gerard, J.; Dejean, C.; Feuillade, J.; Gautier, M.; Montagné, L.; Fuentes, C.; Hannoun-Levi, J. The inverse square law: A basic principle in brachytherapy. *Cancer Radiothér.* **2022**, *26*, 1075–1077. [CrossRef]
37. Turner, J.; Claringbold, P.G.; Klemp, P.F.; Cameron, P.J.; A Martindale, A.; Glancy, R.J.; E Norman, P.; Hetherington, E.L.; Najdovski, L.; Lambrecht, R.M. 166Ho-microsphere liver radiotherapy: A preclinical SPECT dosimetry study in the pig. *Nucl. Med. Commun.* **1994**, *15*, 545–553. [CrossRef]
38. Soares, D.C.F.; de Oliveira, M.C.; dos Santos, R.G.; Andrade, M.S.; Vilela, J.M.C.; Cardoso, V.N.; Ramaldes, G.A. Liposomes radiolabeled with 159Gd-DTPA-BMA: Preparation, physicochemical characterization, release profile and in vitro cytotoxic evaluation. *Eur. J. Pharm. Sci.* **2011**, *42*, 462–469. [CrossRef]
39. Soares, D.C.F.; de Oliveira, M.C.; de Barros, A.L.B.; Cardoso, V.N.; Ramaldes, G.A. Liposomes radiolabeled with 159Gd: In vitro antitumoral activity, biodistribution study and scintigraphic image in Ehrlich tumor bearing mice. *Eur. J. Pharm. Sci.* **2011**, *43*, 290–296. [CrossRef] [PubMed]
40. Galvão, I.; Neves, M.; Santos, R. Evaluation of Gd and Gd 159 as New Approaches for Cancer Treatment. In Proceedings of the International Nuclear Atlantic Conference, Belo Horizonte, Brazil, 24–28 October 2011.
41. Cipreste, M.F.; Peres, A.M.; Cotta, A.A.; Aragón, F.H.; Antunes, A.D.M.; Leal, A.S.; Macedo, W.A.; de Sousa, E.M. Synthesis and characterization of 159Gd-doped hydroxyapatite nanorods for bioapplications as theranostic systems. *Mater. Chem. Phys.* **2016**, *181*, 301–311. [CrossRef]
42. Braat, A.J.; Huijbregts, J.E.; Molenaar, I.Q.; Rinkes, I.H.M.B.; van den Bosch, M.A.A.J.; Lam, M.G.E.H. Hepatic radioembolization as a bridge to liver surgery. *Front. Oncol.* **2014**, *4*, 199. [CrossRef] [PubMed]
43. Dewaraja, Y.K.; Ljungberg, M.; Koral, K.F. Accuracy of 131I tumor quantification in radioimmunotherapy using SPECT imaging with an ultra-high-energy collimator: Monte Carlo study. *J. Nucl. Med.* **2000**, *41*, 1760–1767.
44. Perez-Garcia, H.; Barquero, R. The HURRA filter: An easy method to eliminate collimator artifacts in high-energy gamma camera images. *Rev. Española Med. Nucl. Imagen Mol.* **2017**, *36*, 27–36. [CrossRef]
45. Bouzekraoui, Y.; Bentayeb, F.; Asmi, H.; Bonutti, F. Determination of the energy windows for the triple energy window scatter correction method in gadolinium-159 single photon emission computed tomography using Monte Carlo simulation. *Iran. J. Med. Phys.* **2019**, *16*, 405–409.